Yield-stress fluid deposition in circular channels

Benoît Laborie[1,3,†], **Florence Rouyer**[2], **Dan E. Angelescu**[3,4]
and Elise Lorenceau[1]

[1]Université Paris-Est, Laboratoire Navier, UMR 8205 CNRS, ENPC ParisTech, IFSTTAR,
2 allée Kepler, 77 420 Champs-Sur-Marne, France

[2]Université Paris-Est, Laboratoire Navier, UMR 8205 CNRS, ENPC ParisTech, IFSTTAR,
5 Bd. Descartes 77 454 Champs-Sur-Marne, France

[3]Université Paris-Est, ESIEE Paris/ESYCOM, 2 Bd. Blaise Pascal, 93162 Noisy le Grand, France

[4]Fluidion SAS, 231 Rue St. Honoré, 75001 Paris, France

Since the pioneering works of Taylor and Bretherton, the thickness h of the film deposited behind a long bubble invading a Newtonian fluid is known to increase with the capillary number power 2/3 ($h \sim RCa^{2/3}$), where R is the radius of the circular tube and Ca is the capillary number, comparing the viscous and capillary effects. This law, known as Bretherton's law, is valid only in the limit of $Ca < 0.01$ and negligible inertia and gravity. We revisit this classical problem when the fluid is a yield-stress fluid (YSF) exhibiting both a yield stress and a shear-thinning behaviour. First, we provide quantitative measurement of the thickness of the deposited layer for Carbopol, a Herschel–Bulkley fluid, in the limit where the yield stress is of a similar order of magnitude to the capillary pressure and for $0.1 < Ca < 1$. To understand our observations, we use scaling arguments to extend the analytical expression of Bretherton's law to YSFs in circular tubes. In the limit of $Ca < 0.1$, our scaling law, in which the adjustable parameters are set using previous results concerning non-Newtonian fluids, successfully retrieves several features of the literature. First, it shows that (i) the thickness deposited behind a Bingham YSF (exhibiting a yield stress only) is larger than for a Newtonian fluid and (ii) the deposited layer increases with the amplitude of the yield stress. This is in quantitative agreement with previous numerical results concerning Bingham fluids. It also agrees with results concerning pure shear-thinning fluids in the absence of yield stress: the shear-thinning behaviour of the fluid reduces the deposited thickness as previously observed. Last, in the limit of vanishing velocity, our scaling law predicts that the thickness of the deposited YSF converges towards a finite value, which presumably depends on the microstructure of the YSF, in agreement with previous research on the topic performed in different geometries. For $0.1 < Ca < 1$, the scaling law fails to describe the data. In this limit, nonlinear effects must be taken into account.

Key words: bubble dynamics, coating, non-Newtonian flows

† Email address for correspondence: blaborie@lps.ens.fr

1. Introduction

When a plate or a fibre is drawn out of a liquid bath, a thin liquid film remains on its surface. Similarly, when a long bubble moves into a tube of radius R which is pre-filled with a fluid, a thin layer of liquid remains on the wall of the channel as the bubble displaces the fluid. Finding how h, the thickness of the deposited film, varies with the different parameters driving the deposition of the fluid on solid walls has been extensively studied for various geometries and fluids, and is commonly referred to as 'the coating or deposition problem'.

The deposition of Newtonian fluids, in conditions where gravity and inertia are negligible compared to surface tension and viscous effects, was first investigated in the 1950s by Landau & Levich (1942), Bretherton (1961), Taylor (1961), Cox (1962), who showed that h, the liquid layer deposited in a tube of radius R, scales as:

$$\frac{h}{R} \sim Ca^{2/3}, \tag{1.1}$$

where $Ca = (\eta V / T)$ is the capillary number, V the bubble velocity, η the fluid viscosity and T the liquid–air surface tension. Equation (1.1) is the classical Bretherton's law, which compares remarkably well with experiments for $Ca \ll 1$ (or, equivalently: $(h/R) \ll 1$) (Bretherton 1961; Taylor 1961; Aussillous & Quéré 2000), with a proportionality coefficient of 1.34, which depends on the length of the bubble, as shown by Schwartz, Princen & Kiss (1986). For $Ca \approx 1$, h tends to a finite value $((h/R) \simeq 0.4)$, as shown by Taylor (1961), and later by Cox (1962) and Reinelt & Saffman (1985).

The deposition of non-Newtonian fluids, initially motivated by the development of the photographic industry (Deryagin & Levi 1964), has been widely used in various industrial processes to enhance, modify, or decorate the surface properties of chosen substrates. Indeed, coating materials, such as paints and lacquers commonly used to prevent corrosion in the automotive industry, often behave like non-Newtonian fluids. The deposition of various non-Newtonian fluids, such as polymer solutions or elastic fluids, has been addressed theoretically, numerically or experimentally (Gutfinger & Tallmadge 1965; Huzyak & Koelling 1997; de Ryck & Quéré 1998; Gauri & Koelling 1999; Quéré 1999; Kamisli & Ryan 1999, 2001; Kamışlı 2003; Duggal & Pasquali 2004; Weinstein & Ruschak 2004; Behr *et al.* 2005; Quintella, Mendes & Carvalho 2007; Ashmore *et al.* 2008; Boehm, Sarker & Koelling 2011). In particular, for a shear-thinning or shear-thickening fluid, with a stress/strain-rate relationship in simple shear given by $\tau = k\dot{\gamma}^n$ (where n denotes the power-law index and k the consistency (in Pa s^n)), the same scaling arguments as for Newtonian fluids can be used (Gutfinger & Tallmadge 1965; de Ryck & Quéré 1998; Hewson, Kapur & Gaskell 2009), thus yielding:

$$\frac{h}{R} \sim \widehat{Ca}^{2/(2n+1)}, \tag{1.2}$$

where $\widehat{Ca} = (k(V/R)^n / T / R)$ is a modified capillary number for shear-thinning/thickening fluids, which reduces to Ca for $n = 1$.

The deposition of yield-stress fluids (YSFs) has been investigated in different geometries. Such fluids are characterized by an intermediate fluid or solid behaviour: they exhibit an elastic response below, and liquid flow response above a critical yield stress τ_y. In the geometry of a plate withdrawn from a bath full of YSF, the thickness of the deposited layer was shown to be almost independent of the velocity,

but proportional to the material yield stress (Boujlel & Coussot 2013; Maillard, Boujlel & Coussot 2014). Using particle imaging velocimetry, the authors observe that a uniform boundary layer builds up along the plate before emersion out of the bath. This boundary layer, set by a balance between the yield and gravity stresses, also determines h, the thickness of the deposited layer, so that $h \propto \tau_y$, in good agreement with experimental data. This experimental result differs from earlier theoretical works concerning the deposition of purely plastic materials on a fibre, which predicts that $h \propto \tau_y^2$ (Deryagin & Levi 1964; Quéré 1999). This discrepancy is due to the geometry: the theoretical predictions concern the deposition on a fibre, where the capillary pressure, set by the large curvature of the fibre, is of the same order of magnitude as the yield stress, while in the planar geometry of the plate, the capillary pressure, far smaller than the yield stress, is neglected (Boujlel & Coussot 2013; Maillard *et al.* 2014). In a circular channel, the deposition of YSFs has received relatively little consideration to date, despite its relevance in numerous and diverse applications in industry (e.g. gas-assisted injection moulding (Park *et al.* 2003), channel-cleaning processes in the petroleum or food industries, displacement of hydraulic fracturing fluid (Boronin, Osiptsov & Desroches 2015)) or in biomedical research (reopening of pulmonary airways (Zamankhan *et al.* 2012)). In this confined geometry, the capillary pressure, set by the channel's curvature (typically of 10^4 m^{-1}), competes with the gravity and yield stresses as in the geometry of the fibre. Moreover, in a tube, the flow of the YSF is characterized by an intermediate solid–liquid behaviour (Froishteter & Vinogradov 1980): an elastic solid core appears at the centre of the tube, where the shear stress is less than the yield stress, surrounded by a sheared liquid annulus of thickness e where the shear stress overcomes the yield stress (as sketched in figure 1):

$$e = R - \tau_y L / \Delta P, \qquad (1.3)$$

where L is the length of the tube and ΔP is the pressure drop between the inlet and outlet of the tube. The shape of the liquid/air interface may be altered by this solid-like region of the flow, which in turn could modify the deposition mechanism.

In this article, we report on the deposition of a YSF in circular channels, and provide experimental data obtained in the limit where the capillary pressure is of the same order of magnitude as the yield stress of the fluid. Our data concern channels with various radii and over more than two orders of magnitude of flow velocities. To explain our experimental observations we develop a new scaling model that takes into account the yield stress, the capillary pressure and the viscous stress; it qualitatively describes our experimental data (for $\widehat{Ca} > 0.1$), and is in quantitative agreement with literature data even in the regime $\tau_y \lesssim T/R$, where previously published models are not applicable (for $\widehat{Ca} < 0.1$).

2. Material and experimental set-up

We use a Carbopol gel (980 from Cooper) as our model YSF. Carbopol is made of polyacrylic acid (PAA) resins dispersed in water and neutralized with a base. The neutralization generates ionic repulsion between the polymer chains which adopt an expanded configuration, thus forming blobs that swell until the osmotic pressure inside the blob balances the pressure inside the solvent. The size of individual blobs is of the order of 100 µm (Piau 2007; Mahaut *et al.* 2008). Due to its non-thixotropic behaviour (Coussot *et al.* 2009), Carbopol gel is a good model of a simple YSF.

We prepare the Carbopol solution by dispersing it in water at a concentration of 1.1 % and neutralizing the resulting solution using sodium hydroxide (NaOH,
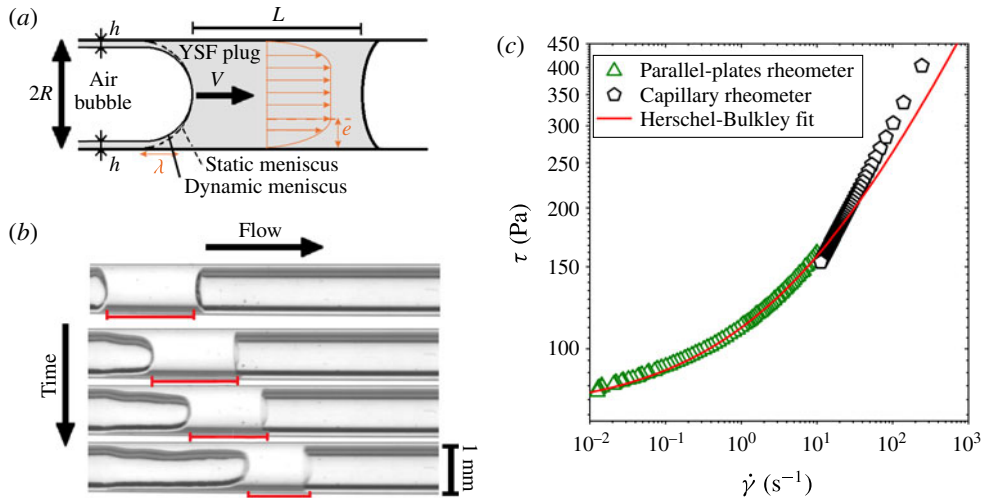
FIGURE 1. (Colour online) (*a*) Sketch of the experiment with the different length scales of the problem highlighted. (*b*) Typical images of a YSF plug as it accelerates during the channel flow for $\tau_y = 70$ Pa, $R = 513$ µm, and an applied pressure $\Delta P = 25$ mbar. The solid lines stand for the measure of $L(t)$. The interval of time between images is equal to 0.33 s. (*c*) Rheogram of the Carbobol gel used in the experiments: stress (τ) versus strain rate ($\dot{\gamma}$). Triangles are obtained with a parallel-plates rheometer, and pentagons are computed from the Mooney–Rabinowitsch formula in a smooth glass capillary ($R = 513$ µm) treated with PEI to avoid wall slip. The solid line represents the Herschel–Bulkley law with $\tau_y = 70$ Pa, $k = 35$ Pa s^n and $n = 0.35$.

1 mol l^{-1}). The mixing lasts 24 hours and is performed with a planetary mixer to ensure an homogeneous mixing throughout the sample. The density (ρ) of the Carbopol solution we used is 980 kg m^{-3}, and its surface tension (T) is 66 mN m^{-1} (Boujlel & Coussot 2013; Jorgensen *et al.* 2015).

Carbopol plugs (of length $L > 2R$) are pushed at constant pressure in glass capillaries (radius $R = 235, 513, 702$ µm). To avoid wall slip (Barnes 1995), our glass capillaries are treated with a solution of polyethylenimine (PEI from Sigma-Aldrich) (Metivier *et al.* 2012). The capillary tubes are cleaned with ethanol, dried, and finally immersed in a PEI solution at 0.2 %wt. in water for 24 h. The pressure is imposed using a Fluigent pressure controller (MFCZ, 0–2 bar, ±2 mbar), and a movie of the experiments is recorded with a camera (AVT Marlin, maximum frame rate 200 fps). The maximum resolution of the camera is 2.82 µm (1 px). Using (2.1) this value leads to a mean error in h of approximately 20 %.

2.1. *Rheological properties of Carbopol gels*

Under simple shear, the rheological properties of Carbopol gels are classically modelled by a Herschel–Bulkley law: $\tau = \tau_y + k\dot{\gamma}^n$ where τ and $\dot{\gamma}$ are respectively the shear stress and the shear rate. Figure 1(*c*) shows a rheogram of a Carbopol gel over a wide range of shear rate. Low shear rates are explored with a parallel-plates rheometer (Bohlin C-VOR, with rough plates of diameter 40 mm) whereas large shear rates are explored using a capillary rheometer (glass capillary of radius $R = 513$ µm) and computed from the Mooney–Rabinowitsch formula (Macosko 1994). The measured

Rheometer	τ_y (Pa)	k (Pa s^n)	n
Parallel-plates rheometer	74	38	0.35
Capillary rheometer	70	35	0.35

TABLE 1. Comparison between rheological properties of Carbopol gels measured by 'classical' rheometry (rough parallel-plates rheometer) and computed from the Mooney–Rabinowitsch formula in a smooth glass capillary ($R = 513$ µm) treated with PEI to avoid wall slip.

values of τ_y, k and n in these two configurations are reported in table 1. In the following we consider that $\tau_y = 70$ Pa, $k = 35$ Pa s^n and $n = 0.35$. The shear modulus of our carbopol gel is obtained by stress–strain-rate measurements, and found to be 100 Pa.

2.2. *Measurement of the film thickness*

We deduce the film thickness (h) from the length (L) of YSF plugs pushed by an air bubble at constant pressure in glass capillaries. As the plug advances inside the capillary, L decreases due to the deposition of the film on the capillary's wall. Its velocity (V) increases in turn due to the decrease in hydrodynamic resistance associated with its flow at the imposed gas pressure (Baudoin *et al.* 2013). This method, used to study the inertial limit of deposition of Newtonian fluids in capillaries (Aussillous & Quéré 2000), allows one to obtain a whole curve $h = f(V)$ in a single experiment. To ensure that dynamical effects are indeed negligible in YSF deposition, we also measure the layer deposited when pushing the gas at constant velocity and check that this stationary measurement coincides with the dynamical one.

The typical velocity of the experiment (V), measured at the rear meniscus of the plug (i.e. the front meniscus of the bubble), typically ranges between 1 mm s^{-1} and 20 cm s^{-1}. A sketch of the experiment, as well as consecutive images of a moving plug are shown in figure 1(*b*). Data of $L(t)$ and $V(t)$ are presented in figure 2(*a*). The length of the plug decreases (respectively the velocity increases) more and more rapidly during the experiment until the plug ruptures. We associate this behaviour with the large viscosity contrast between the fluid and air, as shown by Fujioka, Takayama & Grotberg (2008) and later on by Baudoin *et al.* (2013).

To avoid finite size effects (Fujioka *et al.* 2008; Zamankhan *et al.* 2012), we only consider data for which the length of the plugs (L) satisfies $L > 2R$, i.e. the data in the shaded area of the graphs in figure 2(*a*) are not considered in the following. We report that when $L < 2R$ the film thickness tends to increase rapidly. However, due to the high speed of this regime we were not able to investigate it systematically.

Assuming that the deposit is homogeneous on the channel surface, and that the plug has a cylindrical shape, a mass balance on the moving plug yields:

$$\frac{h}{R} = 1 - \sqrt{1 - \frac{1}{V(t)}\frac{\mathrm{d}L}{\mathrm{d}t}}. \tag{2.1}$$

The deposited thickness (h) is thus deduced from the data presented on figure 2 using (2.1). In (2.1), the film thickness is assumed to be invariant by rotation along the axis of the tube. Yet, it can be seen from figure 1(*b*) that it is not always true; therefore, the determined film thickness is an equivalent mean annular film thickness.
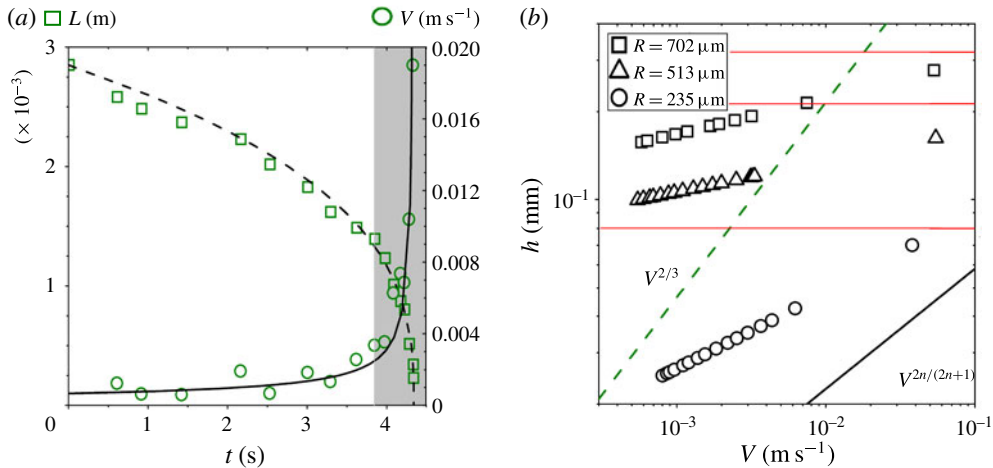
FIGURE 2. (Colour online) (a) Typical experimental data for a YSF plug pushed at constant pressure ($\Delta P = 50$ mbar) in a capillary of radius $R = 702$ µm. Squares: time evolution of the length of the plug (L); circles: time evolution of the velocity of the rear meniscus of the plug (V). The data points in grey area are excluded from the deposition analysis in regards to finite size effects ($L \leqslant 2R$). Solid and dashed lines are fitting functions used to compute equation (2.1). (b) Film thickness (h) deposited by Carbopol plugs ($\tau_y = 70$ Pa, $k = 35$ Pa s^n and $n = 0.35$) as a function of the bubble velocity (V) in capillaries of different radii. Squares: $R = 702$ µm, $\Delta P = 10$ mbar; triangles: $R = 513$ µm, $\Delta P = 20$ mbar; circles: $R = 235$ µm, $\Delta P = 30$ mbar. The dashed line stands for the typical variation of the deposited thickness expected for a Newtonian fluid, and the solid line for the typical variation of the deposited thickness predicted for a shear-thinning fluid with $n = 0.35$ for $R = 1$ mm. The three solid red lines indicate the thicknesses of the sheared layer of YSF in the three tubes deduced from (1.3): $e(R = 702$ µm$) = 0.32$ mm, $e(R = 513$ µm$) = 0.21$ mm, and $e(R = 235$ µm$) = 0.08$ mm; for a given tube's radius, $h < e$.

3. Experimental results

Data obtained using (2.1) for YSF plugs in capillaries of different radii are shown in a log–log plot in figure 2(b) along with the typical power-law variation of the deposited thickness with the velocity predicted by (1.1) and (1.2).

Different features are visible in figure 2(b). First, at a given flow velocity, increasing the radius R results in a larger deposited thickness h. Second, for all capillary radii, h increases like V^x, with x varying between 0.1 for $R = 513$ and 702 µm and 0.3 for $R = 235$ µm. This exponent x is smaller than what is expected for a Newtonian fluid ($x = 2/3$). For the smallest value of R, it is close to $x = 0.4$ – the value expected for a non-Newtonian shear-thinning fluid with the same power-law index ($n = 0.35$) as the Herschel–Bulkley fluid we use (see (1.2)). Moreover, as highlighted by the red horizontal lines of figure 2(b), h is always smaller than e, the sheared liquid layer deduced from (1.3). This suggests that the deposition process is barely affected by the solid core of the flow; indeed, as R decreases, the capillary pressure increases and overcomes the yield stress nearly everywhere in the channel. Thus, the solid core of the flow, characteristic of the YSF, tends to disappear, and the YSF behaves all the more like a shear-thinning fluid when the tube radius is small.
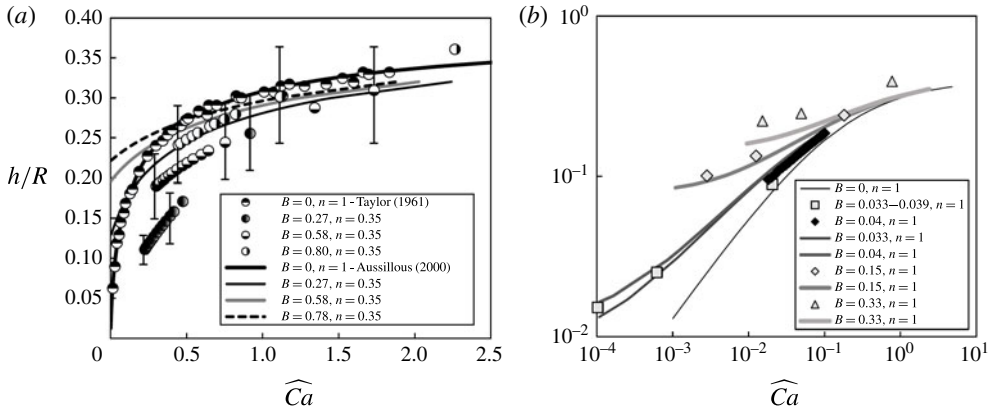
FIGURE 3. (*a*) Normalized film thickness (h/R) as a function of the capillary number $\widehat{Ca}$ for different capillary radii, hence different B. Here, $B = 0.80$ corresponds to $R = 702$ μm, $\Delta P \simeq 10$ mbar, $e/R = 0.46$; $B = 0.58$ to $R = 513$ μm, $\Delta P = 20$ mbar, $e/R = 0.42$; $B = 0.27$ to $R = 235$ μm, $\Delta P = 30$ mbar, $e/R = 0.34$ and $\Delta P = 100$ mbar, $e/R = 0.73$. The symbols obtained by Taylor for different Newtonian fluids (Taylor 1961) are fitted by an empirical expression proposed Aussillous & Quéré (2000) (thick black line). The three other lines (thin black, grey and dash) correspond to (4.7) with $\alpha = 0.33$ and $\beta = 2.4$. (*b*) Computed values of the normalized film thickness as a function of $\widehat{Ca}$ extracted from figure 14 of the work by Zamankhan *et al.* (2012) (full diamonds), and from Jalaal & Balmforth (2016) (open symbols) and fitted for their corresponding values of B and n using (4.7) and $\alpha = 0.33$ and $\beta = 2.4$.

To further compare these results to the classical deposition mechanism for Newtonian fluids, we represent the film thickness h normalized by R as a function of a modified capillary number $\widehat{Ca} = k(V/R)^n/(T/R)$, which takes into account the shear-thinning/thickening part of the non-Newtonian character of the fluid, and compare it in figure 3(*a*) to the data obtained by Taylor (1961) (using viscous fluids with a viscosity η ranging between 0.03 and 0.079 Pa s).

For $\widehat{Ca} < 1$, the thickness of the YSF is smaller than what is expected for a Newtonian fluid. While for $\widehat{Ca} > 1$, it seems to tend to a value close to the Newtonian one. We also report that the data do not collapse on a single curve; which further implies that for a given value of n all the dynamics of the coating process cannot be captured using $\widehat{Ca}$ alone. Since the yield stress of the fluid does not appear in this representation, this deviation is logically attributed to the intermediate solid–liquid behaviour of the fluid, the contribution of which will be highlighted below.

4. Model and discussion

In the following, we first review the deposition laws reported in the literature for different fluids. Then, by adapting the classical model for the deposition of a Newtonian fluid, we propose a new scaling law for the deposition of a YSF.

The case of a Newtonian fluid coating the inside of a circular channel was first considered by Taylor and Bretherton in conditions where gravity and inertia are negligible compared to surface tension and viscous effects (Bretherton 1961; Taylor 1961). In this limit, the deposition process can be understood as follows: the viscous

stresses thicken the film in order to decrease the hydrodynamic resistance associated with the flow in the deposited layer. They also deform the meniscus with respect to its static shape in a region of length λ where the thin film forms. The static and the deformed shape of the interface (also called the dynamic meniscus) are both represented in figure 1(*a*) in solid and dashed lines, respectively. This change of shape generates interfacial stresses, thus leading to a gradient of capillary pressure, scaling like $(1/\lambda)(T/R)$, that counteracts the viscous volumetric forces, scaling like $\eta V/h^2$, with η the fluid viscosity, T its surface tension, and V the velocity of the moving bubble. An analytical solution of this problem was provided by Bretherton (1961) under the lubrication approximation: in the limit where $h \ll \lambda$, matching the curvatures of the static and dynamic menisci provides a second equation for the length of the dynamic meniscus λ:

$$\lambda \sim \sqrt{hR}. \tag{4.1}$$

Combining (4.1) with the balance between the capillary pressure gradient and the viscous effects, the deposition law can naturally be expressed in terms of the capillary number $Ca = (\eta V/T)$, leading to (1.1). In the limit of relative thick film, the radius of curvature of the static meniscus is $R - h$ rather than R, yielding to an expression proposed by Aussillous & Quéré (2000) which fits accurately the experimental data, as can be seen in figure 3(*a*):

$$\frac{h}{R} \sim \frac{Ca^{2/3}}{1 + Ca^{2/3}}. \tag{4.2}$$

The deposition of purely plastic materials of yield stress τ_y and density ρ on a fibre or, respectively, on a plate, has been obtained theoretically by balancing the divergence of the stress tensor τ_y/h with the capillary pressure gradient $(1/\lambda)(T/L_d)$, where L_d is the radius of the fibre or, respectively, the capillary length $\sqrt{T/\rho g}$. Then, using (4.1) (Deryagin & Levi 1964; Quéré 1999) yields:

$$\frac{h}{L_d} \sim B^2, \tag{4.3}$$

where $B = (\tau_y L_d/T)$ is a dimensionless number comparing the yield stress to the capillary pressure.

We emphasize the two following points concerning (4.3). First, equation (4.3) does not depend on flow velocity V, and therefore predicts a deposited film of finite thickness even in the absence of flow. Secondly, equation (4.3) has been derived using (4.1), which is valid only for $(h/\lambda) \ll 1$. Moreover, in terms of length of the dynamic meniscus, equation (4.3) is equivalent to $(h/\lambda) \sim B$. Thus, equation (4.3) cannot be used when the yield stress is of order of the capillary pressure (or equivalently $B \simeq 1$).

Thus, to take into account the different contributions of the capillary, viscous and yield stresses in the limit where $B \simeq 1$, we adapt the classical models for deposition of Newtonian fluids to YSFs. The dimensionless numbers used to characterize the flow and their experimental range of variation are summarized in table 2. Since τ_y is quite large, there is always competition between the yield stress and the capillary pressure jump during the flow of the Carbopol gel in our channels. To compare these two effects, we consider the dimensionless number $B = (\tau_y R/T)$ as suggested by Deryagin & Levi (1964). In our experiment, B is of the order of 1 ($0.27 \leqslant B \leqslant 0.78$). Moreover, the Reynolds and Bond numbers are both $\ll 1$, thus inertial and gravity forces are

$$Re = \frac{\rho V^{2-n} R^n}{k} \quad Bo = \frac{\rho g R^2}{T} \quad \widehat{Ca} = \frac{k\left(\dfrac{V}{R}\right)^n}{T/R} \quad B = \frac{\tau_y R}{T} \quad Bi = \frac{\tau_y}{k\left(\dfrac{V}{R}\right)^n}$$

Range $\quad 10^{-5}$–0.06 $\quad$ 0.008–0.07 $\quad$ 0.2–2.43 $\quad$ 0.27–0.78 $\quad$ 0.31–1.8

TABLE 2. Summary of the dimensionless number used (*Re* for Reynolds, *Bo* for Bond, *Ca* for capillary, *Bi* for Bingham) to characterize the flow and their respective ranges.

negligible compared to viscous forces and surface tension (or the yield stress since $\tau_y \sim (T/R)$). Therefore, the main effects to take into account are: (i) the viscous stresses of the fluid ($k(V/h)^n$ in the dynamic meniscus); (ii) the yield stress of the fluid (τ_y); (iii) the gradient of capillary pressure between the dynamic meniscus ($T/R - h$) and the static meniscus ($2T/R - \beta h$), where β is an adjustable parameter taking into account the non-Newtonian character of the YSF. We now propose a model in the lubrication approximation to take into account our data on the full range of $\widehat{Ca}$. Then, we discuss the physical ingredients of two limiting cases: $\widehat{Ca} \ll 1$ and then $\widehat{Ca} > 1$.

Following Bretherton, we assume that lubrication approximation holds and that the flow is quasi-two-dimensional. Thus, to model the flow dynamics, we simply balance the divergence of the stress tensor and the capillary pressure gradient inside the dynamic meniscus of length λ. This results in (4.4) and its equivalent expression in dimensionless form, equation (4.5):

$$\frac{\tau_y}{h} + \frac{k}{h}\left(\frac{V}{h}\right)^n = \frac{\alpha}{\lambda}\left(\frac{2T}{R - \beta h} - \frac{T}{R - h}\right), \tag{4.4}$$

$$B + \widehat{Ca}\left(\frac{R}{h}\right)^n \sim \frac{h}{\lambda}\left(\frac{2}{1 - \beta\dfrac{h}{R}} - \frac{1}{1 - \dfrac{h}{R}}\right). \tag{4.5}$$

To find the length of the dynamic meniscus λ, we match the curvature $\mathcal{C}_\lambda$ between the static meniscus assuming a shape of spherical cap of radius $R - \beta h$, and the dynamic meniscus of unknown curvature. In the expression above, the fitting parameter β is used to describe an eventual thickening of the film at the bubble apex. We also report that for all moving plugs we are always able to fit the central part of the interface by a circular segment. This suggests that matching the curvature between the spherical cap and the dynamic meniscus is a suitable method to describe our results. Then, using a scaling law equivalent to the one proposed in Aussillous & Quéré (2000) gives:

$$\frac{1}{R - h} + \mathcal{C}_\lambda \sim \frac{2}{R - \beta h}. \tag{4.6}$$

Using (4.5) and (4.6) with $\mathcal{C}_\lambda \sim (h/\lambda^2)$, we compute h, λ as a function of R, B and $\widehat{Ca}$ in (4.7). However, to compare the calculation with the experimental data, we introduce a matching parameter (denoted α). For a Newtonian fluid, this numerical value was determined analytically by Bretherton $\alpha = 1.34$ (Bretherton 1961). For YSFs,

α is unknown, and its numerical computation remains to be done.

$$\widehat{Ca} = \alpha \left(\frac{h}{R}\right)^{n+1/2} \left(\frac{2}{1-\beta\dfrac{h}{R}} - \frac{1}{1-\dfrac{h}{R}}\right)^{3/2} - B\left(\frac{h}{R}\right)^n. \qquad (4.7)$$

We now discuss the different limits of (4.7).

In the limit of $\widehat{Ca} \ll 1$ and considering the flow of a Newtonian fluid ($B = 0$ and $n = 1$), equation (4.7) provides that $(h/R) \ll 1$ and reduces to (1.1) as expected. Then, for a flow of YSF in the limit of vanishing velocity, equation (4.7) reduces to (4.3), which is consistent with the predictions made in the geometry of a fibre when gravity is negligible (Deryagin & Levi 1964; Quéré 1999). In the confined geometry of the tube, this can be understood as follows: in the flow ahead of the bubble, the order of magnitude of the shear rate $\dot{\gamma}$ is V/R, thus in the limit of $\widehat{Ca} \ll 1$, i.e. $k(V/R)^n \ll (T/R)$. Since $(T/R) \sim \tau_y$, τ, the total shear stress given by $\tau = \tau_y + k\dot{\gamma}^n$, is simply $\tau \sim \tau_y$. Therefore, the deposited thickness depends mostly on a balance between the yield stress (τ_y) and the capillary pressure (T/R), i.e. of the dimensionless number $B = (\tau_y R/T)$, in agreement with (4.3).

In the limit of $\widehat{Ca} > 1$, since $B \sim 1$ we expect $Bi = (B/\widehat{Ca}) \ll 1$: the velocity profile along the channel section is Poiseuille-like and the total shear stress $\tau \sim k(V/R)^n$. The deposited thickness is thus expected to saturate towards a constant value, as experimentally observed for Newtonian fluids in figure 3(a) (Taylor 1961) and in shear-thinning fluids (Boehm *et al.* 2011).

Equation (4.7) also allows one to qualitatively determine how the non-Newtonian features of the constitutive equation of the Herschel–Bulkley fluid, i.e. $\tau_y \neq 0$ and $n \neq 1$, influence the deposition process. For a given n and h/R, the larger B, the smaller $\widehat{Ca}$. Thus, for a given value of n the deposited thickness increases with the yield stress. This is valid whatever the value of n: for a given $\widehat{Ca}$, the thickness deposited behind a Bingham fluid is always larger than deposited behind a Newtonian fluid, as shown numerically (Zamankhan *et al.* 2012). We also find that for shear-thinning/thickening fluid (i.e. when $\tau_y = 0$ and $n \neq 1$), h/R is an increasing function of n. The thickness deposited behind a shear-thinning fluid ($n < 1$) is smaller than deposited behind a Newtonian fluid ($n = 1$), itself smaller than deposited behind a shear-thickening fluid ($n > 1$), as previously reported in various works (Gutfinger & Tallmadge 1965; de Ryck & Quéré 1998; Hewson *et al.* 2009). However, the thickness deposited behind a Herschel–Bulkley fluid with $\tau_y \neq 0$ and $n < 1$, or behind a Newtonian fluid $\tau_y = 0$ and $n = 1$, is less straightforward to compare. Equation (4.4) suggests that the yield stress will balance the shear-thinning effects when $\tau_y \sim k(V/h)^n$, i.e. when $B \sim \widehat{Ca}(R/h)^n$, which is equivalently written as $B/\widehat{Ca}(h/R)^n \sim 1$ or $Bi(h/R)^n \sim 1$. Thus, when $Bi(h/R)^n > 1$, the yield stress is dominant and the deposited thickness h/R behind a Herschel–Bulkley fluid is larger than behind a Newtonian fluid, while when $Bi(h/R)^n < 1$, the shear-thinning behaviour dominates and the deposited thickness is smaller than for a Newtonian fluid. This is in agreement with our experiments, which are obtained for large values of $\widehat{Ca}$ for which the shear-thinning behaviour of the fluid is dominant.

We now move to the quantitative comparison of (4.7) and numerical results of the literature. Using a regularized constitutive equation, Zamankhan *et al.* (2012) studied the creeping motion of YSF liquid plugs in two-dimensional channels and computed
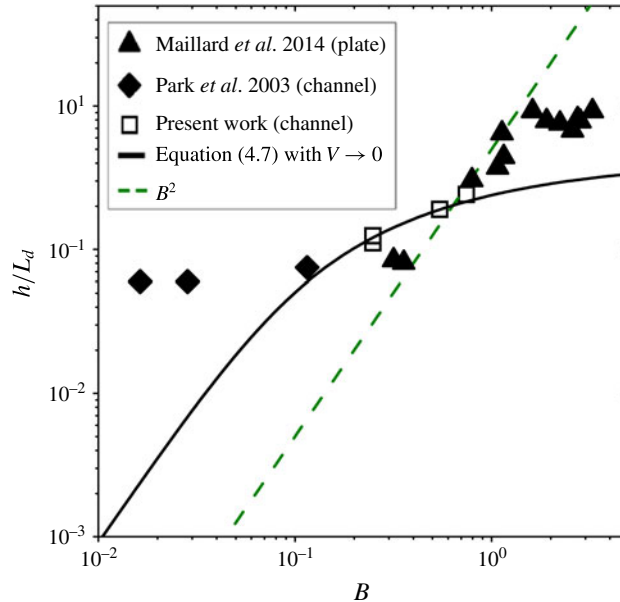
FIGURE 4. (Colour online) Normalized film thickness as a function of $B = (\tau_y L_d / T)$ measured for the smallest accessible velocity for literature results and our experiments: capillaries with $L_d = R = 235, 513, 702 \ \mu m$ and $\tau_y = 70$ Pa (squares – present work); capillaries with $L_d = R = 1.93$ mm and $0.2 \leqslant \tau_y \leqslant 1.5$ Pa (diamonds – Park *et al.* (2003)); withdrawal of plate with $L_d = \sqrt{T/\rho g}$ and $8 \leqslant \tau_y \leqslant 82$ Pa (triangles – Maillard *et al.* (2014)). The green dashed line is a guide for the eye indicating the typical B^2 variation, as in (4.3). The black line stands for (4.7) in the limit of $V \to 0$ with $\alpha = 0.33$ and $\beta = 2.4$.

the evolution of h/R as a function of $\widehat{Ca}$ for Bingham fluids ($n = 1$) and $B = 0.04$. Jalaal & Balmforth (2016) consider Herschel–Bulkley fluids with B in the range of $[0.033 - 0.33]$. Using lubrication theory, they calculate and compute h/R up to value of $\widehat{Ca}$ of the order of 1 by retaining the full surface curvature of the interface, which induces nonlinear effects (Jalaal & Balmforth 2016). In figure 3(*b*), we fit the numerical data of Zamankhan *et al.* (2012) and Jalaal & Balmforth (2016) (chosen for their wide range of $\widehat{Ca}$) using (4.7). By adjusting the fitting parameters of equation (4.7) to their data, which gives $\alpha = 0.33$ and $\beta = 2.4$, we obtain excellent agreement as long as $\widehat{Ca} < 0.01$. For larger values of $\widehat{Ca}$, our expression underestimates the computed values of h/R. We also note that, while the work of Zamankhan *et al.* (2012) consider a parallel plate geometry, it is in good agreement with the work of Jalaal & Balmforth (2016) and the present analytic expression, which are both derived for axisymmetric geometries. This may come from the approximation of an almost two-dimensional flow in the matching region under conditions of sufficiently small values of Ca (Bretherton 1961; Jalaal & Balmforth 2016). Using the same values $\alpha = 0.33$ and $\beta = 2.4$, we compare (4.7) with our experimental data in figure 3*a*. Here also, we fail to describe the data, which is presumably due to the large values of $\widehat{Ca}$ experienced here.

We also focus on the regime independent of the velocity ($V \to 0$). In this regime, h is supposed to depend only on the ratio of the yield stress to the capillary pressure whatever the geometry (plate, fibre, channel), as highlighted by (4.3) and (4.7). Thus, in figure 4, we compare equation (4.7) in the limit of $V \to 0$ to the normalized value

of the first experimentally measurable value of h for (i) Carbopol gels ($\tau_y = 70$ Pa) in tubes (235 µm $< R <$ 702 µm) (our data), (ii) suspensions (0.2 Pa $< \tau_y <$ 1.5 Pa) in tubes ($R = 1.93$ mm) (Park *et al.* 2003) and (iii) Carbopol gels (8 Pa $< \tau_y <$ 82 Pa) on plates using $\sqrt{T/\rho g}$ as the characteristic length (Maillard *et al.* 2014) as a function of B. All data collapse on a single curve that saturates towards $h/L_d \sim 0.07$ when $B \to 0$, increases like B^2 for $0.3 < B < 1$ (as given by (4.3)), and saturates again towards 1 for $B > 1$. Since, (i) the experimental data of this study are not always obtained for completely negligible values of the viscous stress (i.e. $\widehat{Ca} > 0$, which is difficult to achieve experimentally due to the minimum force necessary to overcome the yield stress) and (ii) as underlined previously, the lack of nonlinear terms in the expression of the matching of curvature introducing errors on h when either B and/or $\widehat{Ca}$ approach 1, it is difficult to conclude regarding the apparent good quantitative agreement of the model and the experimental data of this study for $1 < B < 0.1$. However, for $B < 0.1$, the measured values are significantly larger than the prediction: yield-stress fluids possess a microstructure of finite size which may set a minimal value for h when $V \to 0$. Such finite size effects were reported to modify the deposition of dilute emulsions, leading to a saturation of the deposited thickness (Quéré & de Ryck 1998).

5. Conclusion

When there is a competition between the yield stress and the capillary pressure, for a given value of the power-law index (n), the deposition of a YSF in a tube cannot be described by the modified capillary number ($\widehat{Ca}$) alone. In the limit of vanishing $\widehat{Ca}$, the yield stress enhances the deposition (quantified by B), similarly to what is observed in an unconfined geometry (Deryagin & Levi 1964; Maillard *et al.* 2014). Indeed, when the yield stress competes with the capillary pressure, the solid-like nature of the material imposes the deposition of a YSF layer of finite size as the velocity vanishes. The physical process of the deposition with no-slip boundary conditions, when inertial and gravity effects are negligible, is described well by a balance between the internal stresses (yield stress and viscous stress) of the fluid and the capillary pressure gradient. The model we propose is able to predict the initial deposited thickness of numerical data in the literature until the film becomes too thick. For $(h/R) > 0.05$, the expression we use to evaluate the curvature and the lubrication approximation no longer holds. We also underline that an effect of the microstructure of the fluid is expected at low velocity and that, as a consequence, unifying the results obtained with different materials and geometries is a challenge that requires a better understanding of the role of the microstructure and of the various effects (gravity, yield stress, capillary pressure, viscous stress, roughness of the tube).

REFERENCES

ASHMORE, J., SHEN, A. Q., KAVEHPOUR, H. P., STONE, H. A. & MCKINLEY, G. H. 2008 Coating flows of non-Newtonian fluids: weakly and strongly elastic limits. *J. Engng Maths* **60**, 17–41.

AUSSILLOUS, P. & QUÉRÉ, D. 2000 Quick deposition of a fluid on the wall of a tube. *Phys. Fluids* **12**, 2367–2371.

BARNES, H. A. 1995 A review of the slip (wall depletion) of polymer solutions, emulsions and particle suspensions in viscometers: its cause, character, and cure. *J. Fluid Mech.* **56**, 221–251.

BAUDOIN, M., SONG, Y., MANNEVILLE, P. & BAROUD, C. N. 2013 Airway reopening through catastrophic events in a hierarchical network. *Proc. Natl Acad. Sci. USA* **110** (3), 859–864.

BEHR, M., ARORA, D., CORONADO, O. M. & M., PASQUALI 2005 Gls-type finite element methods for visco-elastic fluid flow simulations. In *Proceedings of the third MIT Conference on Computational Fluid and Solid Mechanics*, pp. 586–589.

BOEHM, M. W., SARKER, S. & KOELLING, K. 2011 An experimental investigation of two-phase coating flow within microchannels: the effect of coating fluid rheology. *Microfluid. Nanofluid.* **10** (6), 1175–1183.

BORONIN, S. A., OSIPTSOV, A. A. & DESROCHES, J. 2015 Displacement of yield-stress fluids in a fracture. *Intl J. Multiphase Flow* **76**, 47–63.

BOUJLEL, J. & COUSSOT, P. 2013 Measuring the surface tension of yield-stress fluids. *Soft Matt.* **9**, 5898–5908.

BRETHERTON, F. P. 1961 The motion of long bubbles in tubes. *J. Fluid Mech.* **10**, 166–188.

COUSSOT, P., TOCQUER, L., LANOS, C. & OVARLEZ, G. 2009 Macroscopic versus local rheology of yield stress fluids. *J. Fluid Mech.* **158**, 85–90.

COX, B. G. 1962 On driving a viscous fluid out of a tube. *J. Fluid Mech.* **14**, 81–96.

DERYAGIN, B. V. & LEVI, S. M. 1964 *Film Coating Theory*. The Focal Press.

DUGGAL, R. & PASQUALI, M. 2004 Visualization of individual DNA molecules in a small-scale coating flow. *J. Rheol.* **48**, 745–764.

FROISHTETER, G. B. & VINOGRADOV, G. V. 1980 The laminar flow of plastic disperse systems in circular tubes. *Rheol. Acta* **19** (2), 239–250.

FUJIOKA, H., TAKAYAMA, S. & GROTBERG, J. B. 2008 Unsteady propagation of a liquid plug in a liquid-lined straight tube. *Phys. Fluids* **20**, 062104.

GAURI, V. & KOELLING, K. W. 1999 The motion of long bubbles through viscoelastic fluids in capillary tubes. *Rheol. Acta* **38**, 458–470.

GUTFINGER, C. & TALLMADGE, J. A. 1965 Films of non-Newtonian fluids adhering to flat plates. *AIChE J.* **11** (3), 403–413.

HEWSON, R. W., KAPUR, N. & GASKELL, P. H. 2009 A model for film-forming with Newtonian and shear-thinning fluids. *J. Fluid Mech.* **162**, 21–28.

HUZYAK, P. C. & KOELLING, K. W. 1997 The penetration of a long bubble through a viscoelastic fluid in a tube. *J. Fluid Mech.* **71**, 73–88.

JALAAL, M. & BALMFORTH, N. J. 2016 Long bubbles in tubes filled with viscoplastic fluid. *J. Non-Newtonian Fluid Mech* **238**, 100–106.

JORGENSEN, L., LE MERRER, M., DELANOE-AYARI, H. & BARENTIN, C. 2015 Yield stress and elasticity influence on surface tension measurements. *Soft Matt.* **11**, 5111–5121.

KAMIŞLI, F. 2003 Free coating of a non-Newtonian liquid onto walls of a vertical and inclined tube. *Chem. Engng Process.* **42** (7), 569–581.

KAMISLI, F. & RYAN, M. E. 1999 Perturbation method in gas-assisted power-law fluid displacement in a circular tube and a rectangular channel. *Chem. Engng J.* **75**, 167–176.

KAMISLI, F. & RYAN, M. E. 2001 Gas-assisted non-Newtonian fluid displacement in circular tubes and noncircular channels. *Chem. Engng Sci.* **56**, 4913–4928.

LANDAU, L. & LEVICH, B. 1942 Dragging of a liquid by a moving plate. *ACTA Physicochim. USSR* **17**, 42–54.

MACOSKO, C. W. 1994 *Rheology: Principles, Measurements, and Applications*. Wiley-VCH.

MAHAUT, F., CHATEAU, X., COUSSOT, P. & OVARLEZ, G. 2008 Yield stress and elastic modulus of suspensions of noncolloidal particles in yield stress fluids. *J. Rheol.* **52** (1), 287–313.

MAILLARD, M., BOUJLEL, J. & COUSSOT, P. 2014 Solid-solid transition in landau-levich flow with soft-jammed systems. *Phys. Rev. Lett.* **112**, 068304.

METIVIER, C., RHARBI, Y., MAGNIN, A. & BOU ABBOUD, A. 2012 Stick-slip control of the carbopol microgels on polymethyl methacrylate transparent smooth walls. *Soft Matt.* **8**, 7365–7367.

PARK, C.-S., BAEK, S.-Y., LEE, K.-J. & KIM, S. W. 2003 Two-phase flow in a gas-injected capillary tube. *Adv. Polym. Tech.* **22** (4), 320–328.

PIAU, J. M. 2007 Carbopol gels: elastoviscoplastic and slippery glasses made of individual swollen sponges: meso- and macroscopic properties, constitutive equations and scaling laws. *J. Fluid Mech.* **144**, 1–29.

QUÉRÉ, D. 1999 Fluid coating on a fiber. *Annu. Rev. Fluid Mech.* **31**, 347–384.

QUÉRÉ, D. & DE RYCK, A. 1998 Le mouillage dynamique des fibres. In *Annales de Physique*, vol. 23, pp. 1–149. EDP Sciences.

QUINTELLA, E. F., MENDES, P. R. SOUZA & CARVALHO, M. S. 2007 Displacement flows of dilute polymer solutions in capillaries. *J. Fluid Mech.* **147**, 117–128.

REINELT, D. A. & SAFFMAN, P. G. 1985 The penetration of a finger into a viscous fluid in a channel and tube. *SIAM J. Sci. Comput.* **6** (3), 542–561.

DE RYCK, A. & QUÉRÉ, D. 1998 Fluid coating from a polymer solution. *Langmuir* **14** (7), 1911–1914.

SCHWARTZ, L. W., PRINCEN, H. M. & KISS, A. D. 1986 On the motion of long bubbles in capillary tubes. *J. Fluid Mech.* **172**, 259–275.

TAYLOR, G. I. 1961 Deposition of a viscous fluid on the wall of a tube. *J. Fluid Mech.* **10**, 161–165.

WEINSTEIN, S. J. & RUSCHAK, K. J. 2004 Coating flows. *Annu. Rev. Fluid Mech.* **36**, 29–53.

ZAMANKHAN, P., HELENBROOK, B. T., TAKAYAMA, S. & GROTBERG, J. B. 2012 Steady motion of Bingham liquid plugs in two-dimensional channels. *J. Fluid Mech.* **705**, 258–279.